

Validation and analysis of Earth Radiation Budget active cavity radiometric data (1985-1999)

Jack Paden a, G. Louis Smith b,
Robert B. Lee III c, Kory J. Priestley c,
Dhirendra K. Pandey a, and Robert S. Wilson a

a. Science Applications International Corporation (SAIC)
One Enterprise Parkway, Suite 300
Hampton, VA 23666-5845

b. Virginia Polytechnic Institute and State University (VPI&SU),
NASA Langley Research Center,
Hampton, Virginia 23681

c. NASA Langley Research Center (NASA/LaRC)
Atmospheric Sciences Competency
Hampton, VA 23681

ABSTRACT

On 5 October 1984, the United States' first woman in space, Dr. Sally Ride, inserted the Earth Radiation Budget Satellite (ERBS) into a 57 degree inclined orbit using the shuttles remote manipulator arm. The orbital precession period of the satellite was 72 days. The nonscanner instrument aboard the ERBS has acquired earth-emitted and reflected radiant flux data since that time, having exceeded its designed lifetime of three years by a factor of five. During these 15 years, the ERBS nonscanner has become a de-facto standard to which much remotely sensed radiative flux data is compared. This paper compares the (at present) fifteen year history of the ERBS wide and medium field-of-view nonscanner detectors with the solar irradiance data acquired by the co-located ERBS solar monitor and with the National Climatic Data Center's (NCDC's) earth-surface temperature dataset for the same period.

1. INTRODUCTION

For a period of 15 years, since October 1984, the Earth Radiation Budget Satellite (ERBS) non-scanning active cavity radiometers have measured solar broadband earth-reflected shortwave (0.2 to 5.0 micrometers) and total earth-emitted radiant flux (0.2 to 50 micrometers.) The radiometers were calibrated absolutely on the International Practical Temperature Scale of 1968 [IPTS-68]. The ERBS irradiance measurements are being studied to detect long-term changes in the earth's energy budget and climate temperature changes as indicated by variations in infrared, out-going longwave radiation (OLR). Bush et al¹, have previously discussed the ERBS 13-year dataset (1984-1997.) In this paper we examine the archived 1985-1999, satellite altitude, ERBS wide-field-of-view (WFOV) and medium field-of-view (MFOV) nonscanner active cavity radiometer measurements of the earth and the archived ERBS solar monitor measurements of the solar irradiance as well as the National Climatic Data Center's (NCDC) Monthly Absolute Estimates of Global (land and ocean combined) Temperature Index¹. Fifteen years after its launch, the ERBS non-scanning instrument continues to acquire and transmit data on the earth's radiation budget. During this decade-and-a-half, the ERBE measurements have become a recognized standard for measurements of the earth's OLR^{6,7,8} and reflected shortwave measurements. The ERBS nonscanner data are currently being actively processed, and the measurements are being analyzed and validated at NASA's Langley Research Center (LaRC.)

2. CALIBRATION PROCEDURES

The ERBS active cavity radiometers were calibrated using blackbody radiant fluxes which were modeled using the optical and geometric properties of reference blackbody emitting surfaces and the temperatures measured by IPTS-68

1. http://www.ncdc.noaa.gov/ol/climate/research/1998/anomalies/global_meanT_C.all



platinum resistance thermometers embedded in the blackbodies. In ground vacuum facilities at the manufacturers plant, the radiometers were calibrated on the IPTS-68 temperature-based radiometric scale (using observations of the standard blackbody radiances.) Then the radiometers were used to calibrate the on-orbit standards, consisting of blackbody and tungsten lamp sources built into the radiometer instrumentation. During the on-orbit phases of the ERBS spacecraft mission, the stabilities of the radiometers' responses were assessed from periodic measurements of reference radiances from the flight standards, as well as from direct solar calibrations.

3. SOLAR EXPOSURE OF THE SHORTWAVE FILTER DOME

During the bi-weekly solar calibrations, the WFOV & MFOV shortwave detector filter domes are exposed to direct solar irradiance. The field-of-view angle (axis to limiter) of the ERBS WFOV sensor is 68 degrees (Fig. 1).

Sensor Description	θ_1 (Deg)	θ_2 (Deg)	r_1 (In)	h (In)	r_2 (In)	R_S (In)
ERBS WFOV	68	71.4	0.125	0.500	1.362	1.451
ERBS MFOV	37	44.2	0.125	1.135 (1.308)*	0.980	1.500
Solar Port WFOV	4.1	8.8	0.125	3.022	0.343	--
Solar Port MFOV	3.3	6.97	0.125	3.831	0.343	--

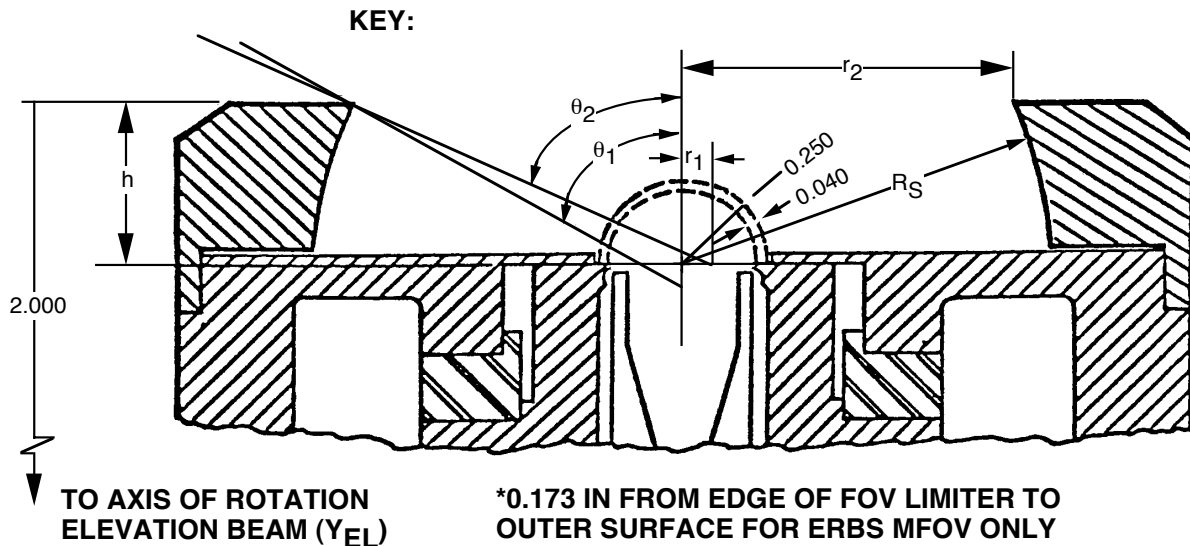


Figure 1. ERBS Nonscanner Specifications & Key

At ERBS altitude, the radius of the earth disk is less than 66° ; therefore, there exists a more than 2 degree annular ring of space surrounding the earth disk. Under numerous orbital conditions, the sun is present in this ring, and therefore the WFOV nonscanner sensors are exposed to full solar irradiance when this occurs (these events will later be referred to as "sunblips."²) Early in the lifetime of the ERBS nonscanner, it became obvious that severe degradation of the WFOV shortwave (SW) channel measurements was occurring. Similar degradation had been noticed in the Nimbus-7 data by Kyle et al³. For the first two-and-a-half years, this ERBS shortwave degradation appeared to be a simple exponential decay effect, but continued observations (Fig. 2) showed it to be much more complex. After the

initial decline, the degradation was flat for about 6 months, then it appeared to “recover” for a month or so, then it again resumed its degradation; but at a slower rate than for the first two and a half years. Degradation of the optics aboard the Earth Radiation Budget (ERB) Nimbus 6 & 7 platforms was previously discussed by Kyle et al², Predmore et al³; and later, Lee et al⁴ discussed the degradation of the ERBE shortwave Suprasil W1 quartz filters.

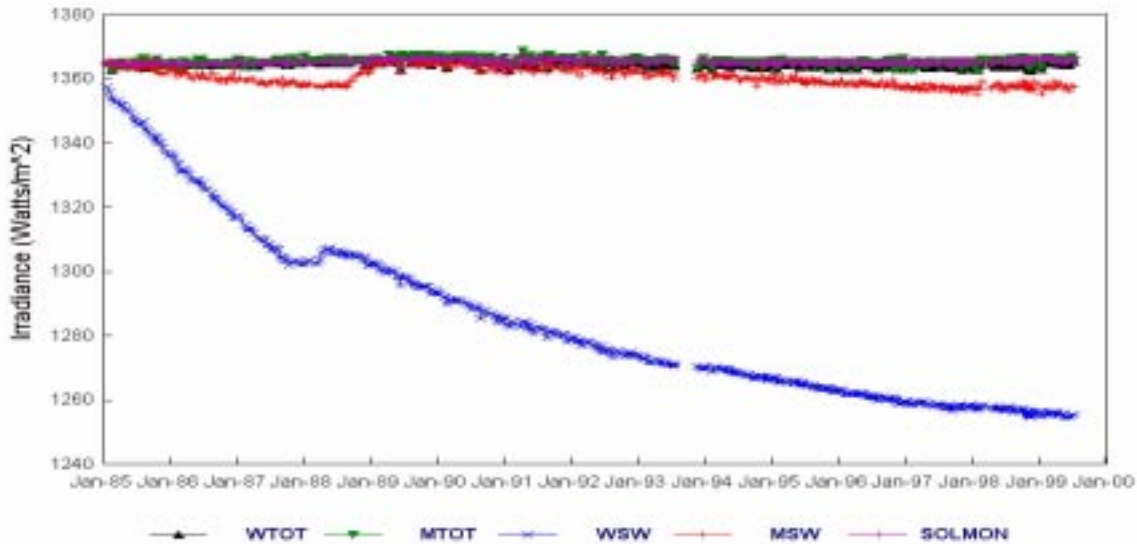


Figure 2. 15-years of ERBS Nonscanner Irradiance Measurements during Solar Calibration Periods

While there was also some degradation in the MFOV shortwave measurements due to the exposure of the filters during bi-weekly solar calibration measurements, this was much less than the WFOV degradation. This is true because the WFOV sensor is subject to much greater radiant exposure when the sun is present in the annular ring of space surrounding the earth disk. When ERBS/Sun orbital conditions are at their worst, “sun-blips” may occur as many as 30 times a day (sunrise and sunset for 15 orbits/day.) The MFOV detector is not subject to any direct solar observations during normal earth-viewing operations because its field-of-view is only 37°. Its filter is therefore never exposed directly to the sun, and hence its degradation is very much less than the WFOV detector.

The ERBS solar calibration sequence, along with the ERBS internal calibration sequence, was performed on a bi-weekly basis during which the ERBS solar monitor detectors measured the incident solar flux. We used the ratio of the SW sensor measurements on the initial solar calibration day to the linearly interpolated value determined by the sensor on the two solar calibration days immediately surrounding the observation day, as a multiplier for the SW counts to linearly compensate for the degradation of the SW filters; thereby effectively adjusting the gain terms for the shortwave measurements to correct for degradation in the transmissivity of the SW filters^{5,6}. We refer to these ratios as “degradation coefficients.”

4. TOTAL, SHORTWAVE, AND DERIVED LONGWAVE MEASUREMENTS

In this paper we chose to limit ourselves to a discussion of longwave (5.0 to 50.0 micrometers) and shortwave (0.2 to 5.0 micrometers) daytime radiant fluxes at a satellite altitude of 611 kilometers. We defined the longwave radiant flux as the difference between the total channel and the shortwave channel measurements. The “true” anomalies for all of the measurements used in this paper are calculated as the difference between the 15-year mean value of the measurements and each individual measurement in the dataset; the difference is then divided by the maximum difference value contained in the dataset. This definition produces “normalized,” dimensionless values (maximum range of ± 1.0), which allow the intercomparison of trends of the separate datasets without regard to their units of measure-

ment. We further restricted ourselves to the daytime measurements (because there is no shortwave flux contribution at night) taken when the solar zenith angle (SZA) was less than, or equal to, 90° (i.e., the daytime measurements.) The ERBS data represent monthly averages of the individual daily averages of all ERBS nadir-viewing measurements. Tabulating the raw data for all four parameters in terms of mean, maximum, minimum, and range about the mean, we obtained the numbers shown in Table 1.

Table 1: ERBS Nonscanner Daytime Flux & Surface Temperature Statistics (1985-1999)

Parameter	Mean	Max	Min	Range from Mean
WFOV LW (w/m ²)	202.97	215.34	191.99	+12.37 to -10.98
MFOV LW (w/m ²)	105.42	112.95	96.77	+7.54 to -8.65
Surface Temp. (deg C)	14.20	16.49	12.1	+2.29 to -2.11
Solar Irrad. (w/m ²)	1365.27	1366.95	1364.0	+1.67 to -1.27

We would like to call attention here to the somewhat complicated spatial geometry involved in the analysis (or visualization) of the ERBS averaged radiant flux data. All of the seasonal references in the following discussion are based on the Northern Hemisphere. At summer solstice the sun is directly over the Tropic of Cancer (23.5°N); at both the vernal and autumnal equinoxes the sun is directly over the equator; and at winter solstice the sun is directly over the Tropic of Capricorn (23.5°S). Therefore, in the summer months, darkness prevails over much of the earth from the Antarctic Circle (66.5°S) to the South Pole. In winter, darkness prevails over much of the region from the Arctic Circle (66.5°N) to the North Pole. Therefore, in the summer ERBS sees less daylight at its southernmost orbital excursion (57°S) but sees more daylight at its northernmost excursion (57°N). Conversely in winter, ERBS will see less daylight at 57°N but sees more daylight at 57°S . At the equinoxes, the earth is evenly illuminated from pole to pole. Fig. 3 shows a 2-dimensional graphic version of this description. For the consideration of averages, as we are doing in this paper, one must also bear in mind that the Northern Hemisphere is predominantly filled with land masses as opposed to the Southern Hemisphere which is mostly oceanic; land masses warm and cool more quickly than oceans; and land masses tend to sustain snow and ice in the winter months. The ERBS WFOV detector sees about 4% of the earth's surface at all times, while the MFOV detector only sees about 0.1%. Consequently, the ERBS MFOV detector does not see the polar areas of either hemisphere at any time of the year. The ERBS WFOV detectors only see into the polar areas when its orbital excursions are in excess of about 42°N or S . The total percentages of the earth's surface which the WFOV and MFOV instruments can observe (at the equinoxes, without accounting for polar oscillation) are 98.85% and 87.6% respectively. These ideas will be applied later (in section 5) when we discuss the analysis of the trends of ERBS radiometric fluxes over the 15-year period.

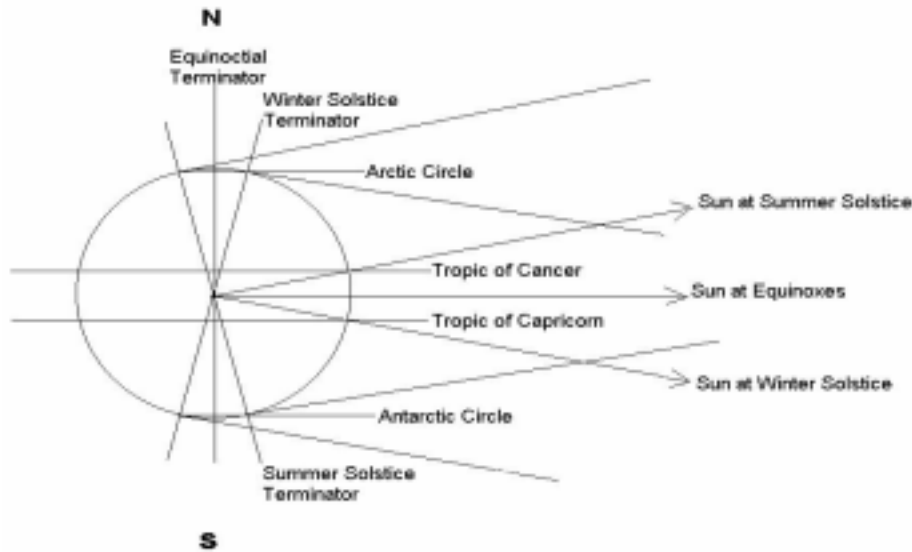


Figure 3. Solar Illumination of the Earth

5. RESULTS AND DISCUSSION

The ERBS derived OLR for the WFOV and MFOV measurements were determined as the difference between the total and the shortwave measurements. The solar monitor channel measurements were acquired along with the measurements of the solar irradiances by the four ERBS nonscanner sensors, during the bi-weekly calibrations. We compare the ERBS solar monitor (irradiance) measurements to the NCDC global average surface temperature data in [Fig 4](#). The 11-year solar cycle is evident in the irradiance data, and there appears to be evidence of the Mt. Pinatubo

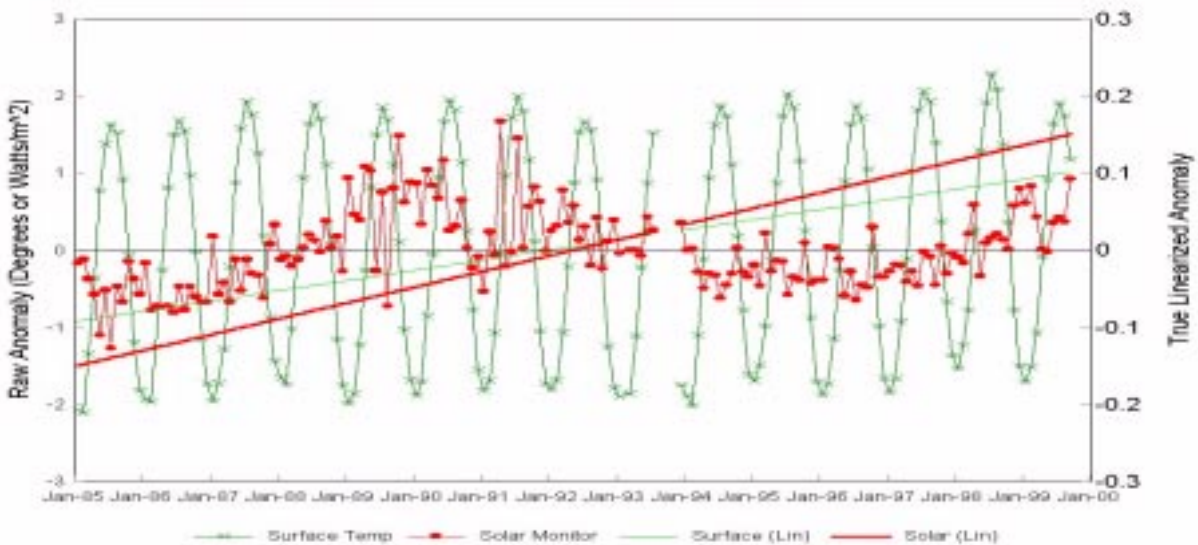


Figure 4. ERBS Solar Irradiance and Surface Temperature Anomalies

eruption^{12,13} in 1991 in the surface temperature data. The linearized trends for both are positive over the interval; however we should also note that computation of the linear trend over the 15-year interval causes some aliasing of the 11-year solar cycle into the trend! An additional note here is that the ERBS nonscanner was “stowed” (turned off) on 1 August 1993 to investigate an anomalous battery condition. On 30 November 1993, when the problem was somewhat better understood, the ERBS was again re-activated in it’s normal “nadir-viewing” mode, and data acquisition continued. The lack of data for this four month period is the reason for the conspicuous gaps in the accompanying figures.

In Fig. 5, we compare the WFOV and MFOV LW anomaly measurements over the period. Once again, the trend is positive for both. The surface temperature anomaly is also plotted for the comparison of orbital effects. The effects of the 1991 Mt. Pinatubo eruption can be seen in the data for 1992 and 1993. Notice that the surface temperature correlates positively with the WFOV and MFOV LW flux anomalies. In Fig. 6, we show the WFOV and MFOV SW data.

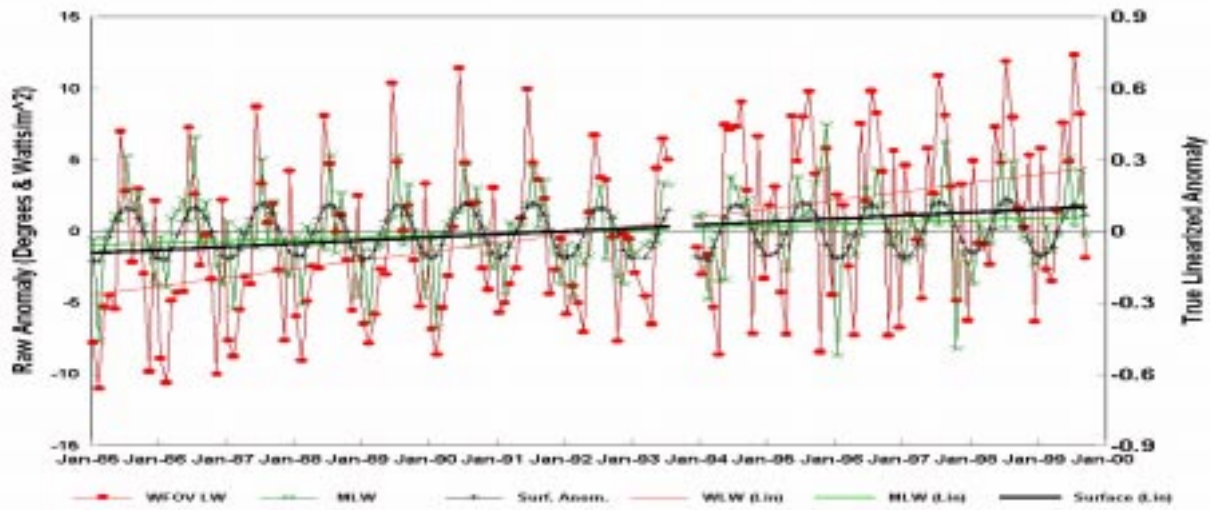


Figure 5. ERBS WFOV & MFOV LW Anomalies

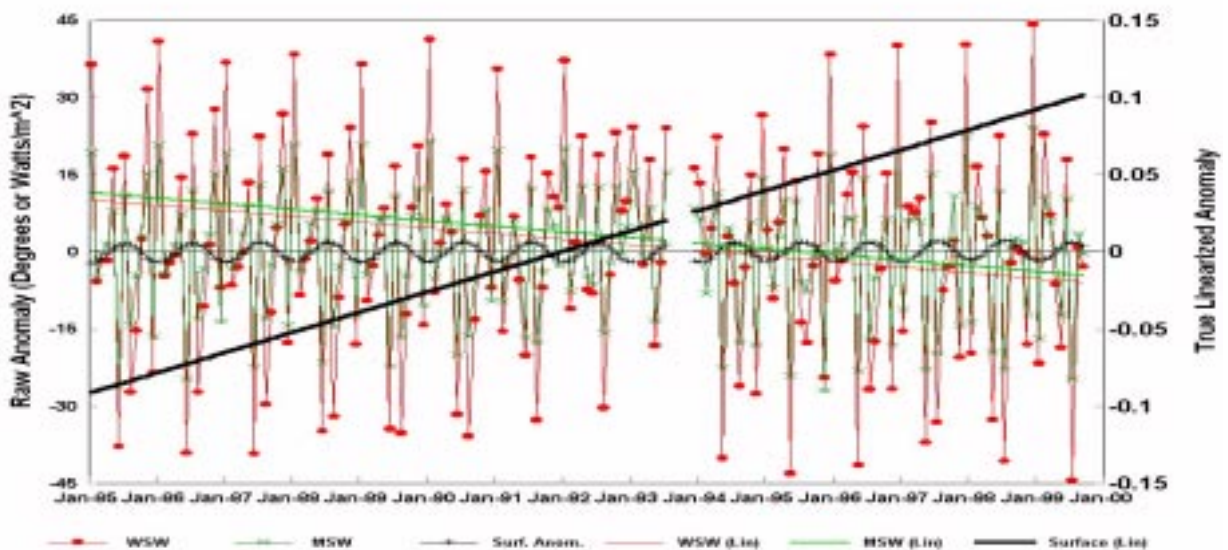


Figure 6. ERBS WFOV & MFOV SW Anomalies

In these cases, the trend is negative (and parallel.) The presence of an atmospheric disturbance prior to 1992 can be seen in this data as well. Notice that the surface temperature correlates negatively, rather than positively, with the WFOV and MFOV SW data. This is at least partly due to the fact that we have defined the LW flux as the difference between the total and SW components. The fact that the linearized anomalies are parallel makes us confident that we have properly corrected the WFOV SW flux for solar degradation of the SW filter dome.

In **Figures 7 & 8**, we display all raw and true anomalies (total, derived LW, and SW) for the WFOV & MFOV detectors, respectively. We have done this to illustrate the relationships between the three spectral ranges covered by each

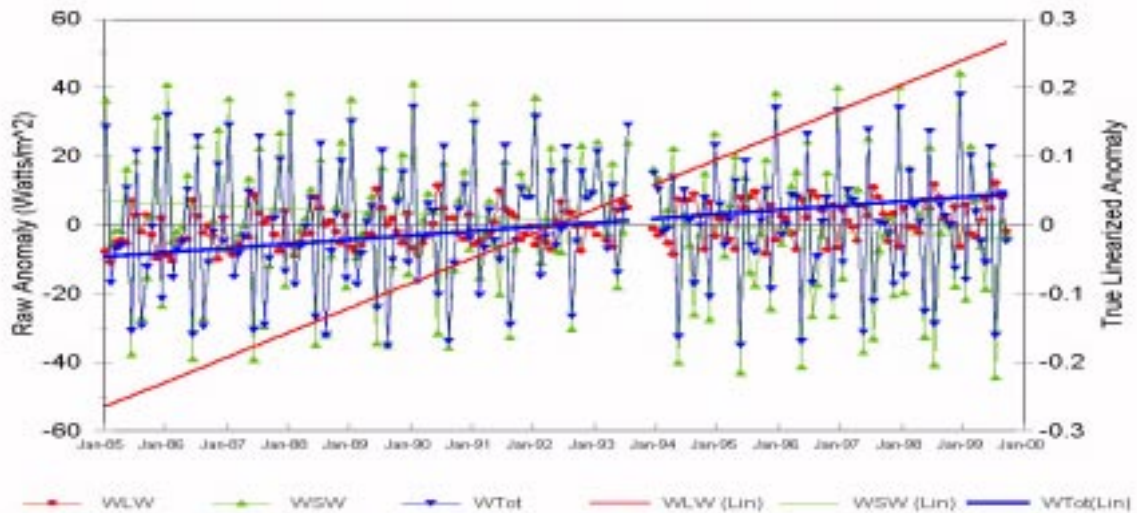


Figure 7. All ERBS WFOV Raw and Linearized Anomalies.

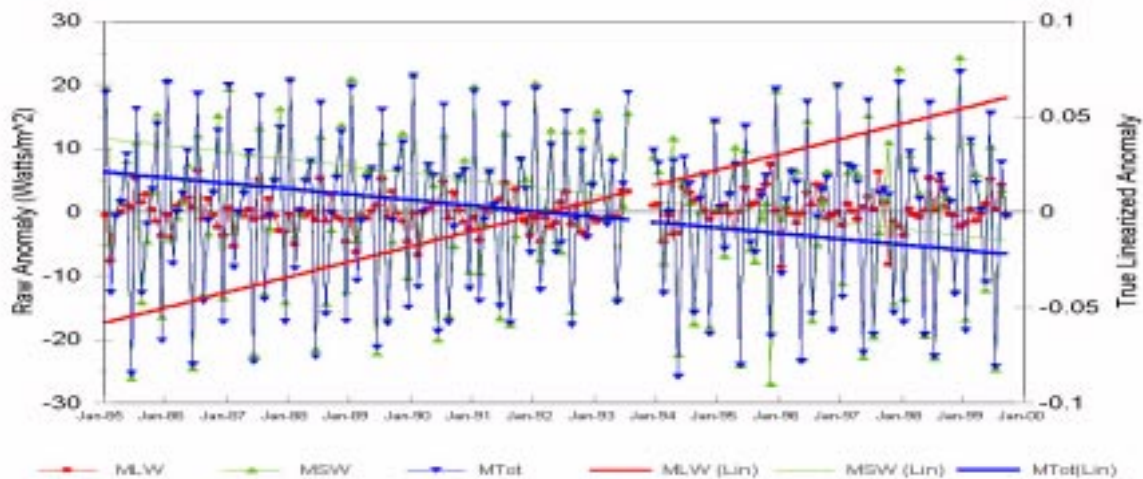


Figure 8. All ERBS MFOV Raw and Linearized Anomalies.

detector. There are approximately 5400 ERBS records per day. Each of the nonscanner detectors were sampled 20 times in each record, yielding a total of 108000 nonscanner samples per channel per day. Using only daytime measurements halves that to 54,000 samples per channel per day. Therefore, over the course of 15 years, the curve for each channel, and each number in Table 1 above, represents the average of approximately 296 million samples

The anomaly plots (Figs. 4-6) are all in very good agreement, showing almost identical annual cyclic variations; and additionally displaying a slight but noticeable increase in the values for longwave flux, surface temperature, and solar irradiance over the 15-year period. While almost flat, the shortwave flux decreased very slightly over the same period. The frequency of the WFOV and MFOV sensor anomalies and the NCDC surface temperature anomaly agreed very well. The correlation of the surface temperature with the LW radiance anomaly was positive, while the correlation of the temperature with the SW anomaly was negative. The data shows that the LW flux peaks during summer in the northern hemisphere; and the SW peaks during winter in the northern hemisphere. We interpret the increase of LW during the northern hemisphere summer as being due to the solar heating of (and the associated emission from) the much larger land masses in the northern hemisphere; and we attribute the increase of SW during northern hemisphere winter as being due to the high snow cover albedo over the larger land masses during the winter. The linear fits of all of the anomalies over the 15-year period verifies that there are slight increases in the WFOV total flux and the WFOV & MFOV LW fluxes, a slight decrease in the WFOV & MFOV shortwave fluxes, and the MFOV total flux. In Figures 6&7, where all WFOV & MFOV anomalies are shown, we are puzzled by the fact that the MFOV total flux decreases while the WFOV total increases, but the fact remains that the LW flux for both WFOV and MFOV sensors increases. The MFOV LW flux increases because the SW flux decreases faster than the total flux, even though the total flux is decreasing. A separate regression (Fig. 9) of the WFOV & MFOV LW nighttime (i.e., the Total channel measurements) data confirmed that the nighttime flux also increased over the 15-year period, thus eliminating the possibility that daytime gains would be diminished by nighttime losses. We note here that the MFOV LW nighttime flux was essentially “flat” over the period and that the true linearized anomaly for the WFOV LW is essentially parallel to that for the surface temperature.

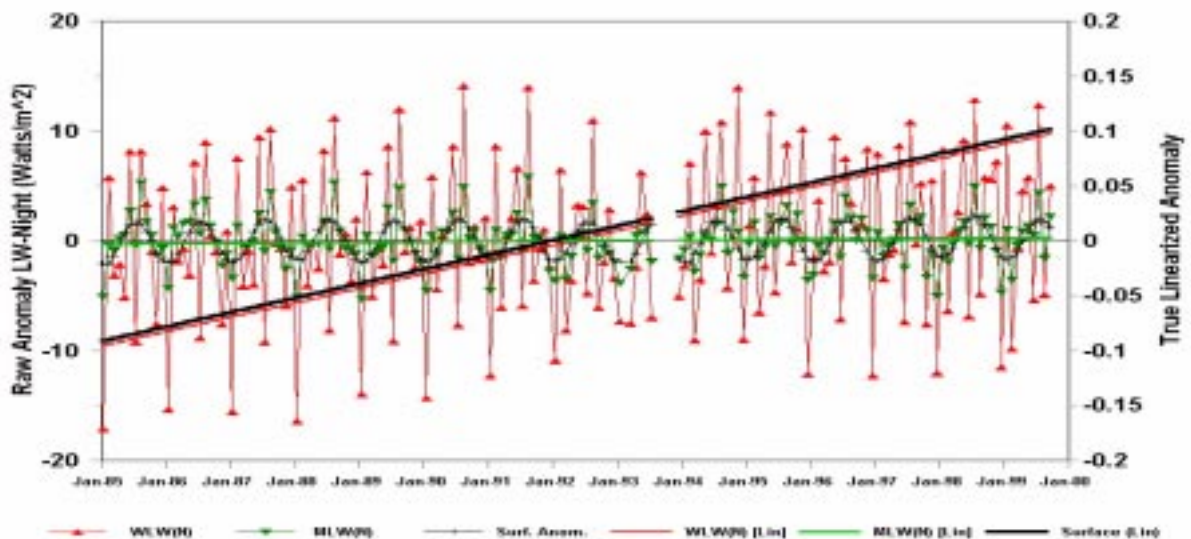


Figure 9. WFOV & MFOV LW Nighttime Fluxes

An obvious question which arises is: “Is the increase in incident solar energy over the period solely responsible for the increase of the OLR?” For the recorded minimum surface temperature of 12.1 degrees Celsius (1985), the equivalent blackbody flux would be 373.66 w/m², and for the maximum surface temperature of 16.49 degrees Celsius (1998), the flux would be 399.04 w/m² (assuming an emissivity of 1.0 for the earth’s surface.) The range of 25.36 w/m² compares fairly well with the 23.35 w/m² range determined from the WFOV channel. The ratio (MFOV/WFOV)

of the means of the LW measurements is 0.52. This ratio when multiplied by the WFOV range of 23.35 w/m^2 yields 12.08 w/m^2 , which is about 4 w/m^2 less than the 16.18 w/m^2 range measured by the MFOV sensor. We note here that an emissivity of 0.9 was used for the ERBS nonscanner blackbodies. The total range of the solar constant over the 15-year period was only 2.95 w/m^2 , but because of the involvement of three orbiting bodies (earth vs. sun, ERBE vs. sun, and ERBE vs. earth), as well as the discussion of the solar illumination of the distinctly variable earth surface throughout the year in section 4 above, we did not attempt to correlate the range in solar output with the ranges of the flux and surface temperature measurements indicated by the other three variables.

6. CONCLUSION

Using the 15-year (1985-1999) WFOV LW flux as the basis, we calculated a mean flux level of 202.97 watts/m^2 . The linearized anomaly for this dataset indicates a range of 199.69 watts/m^2 to 206.12 watts/m^2 (Fig. 10). Using the integrated Planck function blackbody equivalents we obtained temperatures of 243.638 and 245.574 °C, respectively. The averaged rate of increase was therefore the equivalent of 0.13 °C per year, or 13 °C per century, but this would

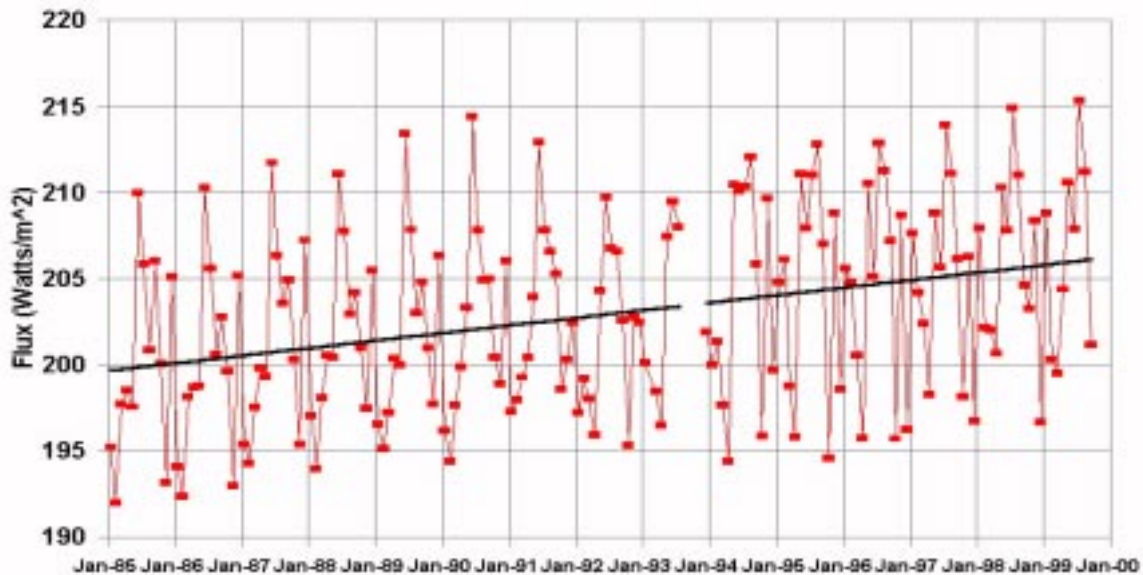


Figure 10. ERBS WFOV LW Flux with Linear Fit

only be true if the 15-year trend continued throughout the next century. We do not have sufficient data to indicate that the trend will continue. Therefore, we neither hypothesize, nor suggest, that this dataset demonstrates a long-term “global-warming” trend. However, we have demonstrated that the data shows a significant warming trend over the 15-year period during which these ERBS nonscanner measurements were acquired.

7. ADDENDUM

To date the ERBS nonscanner radiometers continue to acquire good earth fluxes while the solar monitor continues to provide the longest continuous spacecraft dataset of total solar irradiance measurements. Since 6 October 1999 the nonscanner radiometers have not been calibrated because they cannot be commanded to either the solar views or the internal blackbody/tungsten lamp calibration position. The nonscanner elevation mechanism failed in the nadir position where the radiometer can continue to measure the earth-reflected SW fluxes and the earth-emitted LW fluxes. We performed a comprehensive analysis of the data on each side of 6 October 1999 which indicates that the nonscanner sensors are located within 0.5 degree of the nadir position. Therefore, we are continuing to process the ERBS data,

and are validating the results. We believe that the continued analysis and validation of data acquired by the ERBS nonscanner will provide valuable, additional, long-term historical record of ERB data. The ERBS dataset combined with the previously acquired ERB/Nimbus-6/Nimbus-7 dataset (which dates back to 1975) constitutes a continuous 25-year history of the earth's radiative flux, against which many other atmospheric research measurements are regularly compared^{2,8,9,10,11,12,13}.

8. ACKNOWLEDGEMENTS

This work was supported by the Earth Science Enterprise of NASA through Langley Research Center by contract NAS 1-19570 with SAIC and cooperative agreement NCC-1-405 with VPI&SU.

9. REFERENCES

1. Kathryn A. Bush, G. Louis Smith, David A. Rutan, Bruce R. Barkstrom, R. B. Lee, III, and David Young, "The Earth Radiation Budget Satellite 13-Year Data Set," AMS 10th Symposium on Global Change Studies, 504-507 (1997)
2. H. Lee Kyle, R. Hucek, Philip Ardanuy, Lanning Penn, Brian Groveman, John Hickey, and Robert Maschoff, "In-flight Calibration of the Nimbus-7 Earth Radiation Budget (ERB) Sensors, Part II: Short-Term Perturbations," Journal of Atmospheric and Oceanic Technology, Vol. 12, No. 6, 1150-1162 (1995).
3. R. E. Predmore, H. Jacobowitz, and J.R. Hickey, "Exospheric cleaning of the Earth Radiation Budget solar radiometer during solar maximum," Proc. Soc. Photo-Opt. Instrum. Eng., 338, 104-113 (1982).
4. R. B. Lee III, L. M. Avis, M. A. Gibson, S. Thomas, and R. Wilson, "In-flight Evaluations of Tungsten Calibration Lamps Using Shortwave Thermistor Bolometers and Active-cavity Radiometers," Metrologia, 30, 389-395 (1993).
5. J. Paden, D. K. Pandey, R. Wilson, S. Thomas, M. A. Gibson, and R. B. Lee III, "Ground and in-flight calibrations for the earth radiation budget experiment (ERBE) non-scanning radiometers," in Remote Sensing of the Biosphere, Proc. Soc. Photo-Opt. Instrum. Eng., 1300, 190-201 (1990).
6. R. Wilson, W. C. Bolden, M. A. Gibson, R. B. Lee III, J. Paden, D. K. Pandey, and S. Thomas, "In-flight Calibration of Shortwave Active Cavity Radiometers: Approach and Results," in Recent Advances in Sensors, Radiometric Calibration, and Processing of Remotely Sensed Data, Proc. Soc. Photo-Opt. Instrum. Eng., 1938, 2-10 (1993).
7. H. L. Kyle, J. R. Hickey, P. E. Ardanuy, H. Jacobowitz, A. Arking, G. G. Campbell, F. B. House, R. Maschoff, G. L. Smith, L. L. Stowe, and T. Vonder Haar, "The Nimbus Earth Radiation Budget (ERB) Experiment: 1975 to 1992," Bul. Am. Met. Soc., Vol. 74, No. 5, 815-830 (1993).
8. T. Dale Bess and G. Louis Smith, "Earth Radiation Budget: Results of Outgoing Longwave Radiation from Nimbus-7, NOAA-9, and ERBS Satellites," Journal of Applied Meteorology, Vol. 32, No. 5, 813-824 (1993)
9. H. Lee Kyle, Mitchell Weiss, and Philip Ardanuy, "Cloud, Surface Temperature, and Outgoing Longwave Radiation for the Period from 1979 to 1990," Journal of Climate, Vol. 8, No. 11, 2644-2658 (1995).
10. R. B. Lee III and R. S. Wilson, "Validation of 1985-1997 active cavity radiometer spacecraft measurements of total solar irradiance variability," Earth Observing Systems III, Proc. Soc. Photo-Opt. Instrum. Eng., 3439, 377-388 (1998).
11. B. A. Wielicki, T. Wong, D. F. Young, B. R. Barkstrom, R. B. Lee III, and Martial Haeffelin, "Differences between tropical mean fluxes: ENSO, climate change or calibration?," AMS 10th Conf. on Atm. Rad., Madison, WI, June 28-July 2 1999.
12. P. Minnis, E. F. Harrison, L. L. Stowe, G. G. Gibson, F. F. Denn, D. R. Doelling, and W. L. Smith Jr., "Radiative Climate Forcing by the Mount Pinatubo Eruption," Science, Vol. 259, 5 March 1993.



13. D. K. Pandey, R. B. Lee, J. Paden, R. S. Wilson, and S. Thomas, "1984-1999 Inferred Global Earth Atmospheric Temperature Trends From Earth Radiation Budget Satellite (ERBS) Active Cavity Radiometric Measurements," AGU 1999 Fall Meeting, AGU Vol. 80, Number 46, F146, 16 November 1999.

Further author information:

J.P.(correspondence): email: j.paden@larc.nasa.gov; WWW: <http://earth-www.larc.nasa.gov/~jack/>;
Telephone: 757-827-4880; Fax: 757-825-9129

D.K.P.: email: d.k.pandey@larc.nasa.gov; Telephone: 757-827-4890; Fax: 757-825-9129

R.B.L.: email: r.b.lee@larc.nasa.gov; Telephone: 757-864-5679; Fax: 757-864-7996

K.J.P.: email: k.j.priestley@larc.nasa.gov; Telephone: 757-864-8147; Fax: 757-864-7996

G.L.S.: email: g.l.smith@larc.nasa.gov; Telephone: 757-864-5678; Fax: 757-864-7996

R.S.W.: email: r.s.wilson@larc.nasa.gov; Telephone: 757-827-4881; Fax: 757-825-9129

